Letter

Interaction-driven first-order and higher-order topological superconductivity

Pietro M. Bonetti,[1,*] Debmalya Chakraborty ,[2,*] Xianxin Wu ,[3] and Andreas P. Schnyder [1,4]

[1]*Max Planck Institute for Solid State Research*, Heisenbergstrasse 1, D-70569 Stuttgart, Germany
[2]*Department of Physics and Astronomy, Uppsala University, Box 516, S-751 20 Uppsala, Sweden*
[3]*Institute for Theoretical Physics*, Chinese Academy of Sciences, Beijing, China
[4]*Yukawa Institute for Theoretical Physics (YITP), Kyoto University, Kyoto 606-8502, Japan*

We investigate topological superconductivity in the Rashba-Hubbard model, describing heavy-atom superlattice and van der Waals materials with broken inversion. We focus in particular on fillings close to the van Hove singularities, where a large density of states enhances the superconducting transition temperature. To determine the topology of the superconducting gaps and to analyze the stability of their surface states in the presence of disorder and residual interactions, we employ an fRG + MFT approach, which combines the unbiased functional renormalization group (fRG) with a real-space mean-field theory (MFT). Our approach uncovers a cascade of topological superconducting states, including A_1 and B_1 pairings, whose wave functions are of dominant p- and d-wave character, respectively, as well as a time-reversal breaking $A_1 + iB_1$ pairing. While the A_1 and B_1 states have first-order topology with helical and flat-band Majorana edge states, respectively, the $A_1 + iB_1$ pairing exhibits second-order topology with Majorana corner modes. We investigate the disorder stability of the bulk superconducting states, analyze interaction-induced instabilities of the edge states, and discuss implications for experimental systems.

Topological superconductors (TSCs) are of high current interest due to their exceptional properties and potential for applications in quantum information technologies [1–7]. A variety of heterostructures [7] and candidate materials [8–11], where topological superconductivity is expected to occur, have been investigated. However, despite tremendous efforts, the ideal topological superconductor suitable for the envisioned applications has yet to be found. Two major obstacles in this research field are small superconducting gaps and omnipresent disorder. Since the topology only protects against perturbations smaller than the superconducting gap, it is of paramount importance to find intrinsic topological superconductors with larger gaps compared to proximity-induced superconductors [12,13].

Finding intrinsic topological superconductivity needs superconductivity to be originating from electron-electron repulsive interactions since electron-phonon interactions commonly only give conventional nontopological superconductivity [14,15]. One possible path to high-T_c topological superconductivity is to search for platforms using high-T_c cuprate superconductors, for example, as proposed in twisted bilayer cuprates [16]. However, the lack of tunability in material control of cuprates has made it hard to experimentally realize twisted bilayers of cuprates. An alternative strategy investigated in recent times is to use a large density of states at the Fermi level [17]. This strategy has been envisaged in material candidates where the Fermi level lies close to a van Hove singularity [18] or near flat bands [19]. However, a major hindrance towards such possibility of superconductivity is that a large density of states is also associated with particle-hole orders, like ferromagnetism, due to the Stoner criterion [20] or spin/charge density waves due to nesting [21,22]. However, doping away from a ferromagnetic phase to its critical point can result in triplet topological superconductivity, due to ferromagnetic fluctuations [23]. However, the resulting triplet superconductivity is highly fine-tuned, exists only in a narrow region of parameter space, and has an exponentially small T_c, due to the large distance from the singular density of states [24].

Another ingredient which is often believed to be crucial for topological superconductivity is spin-orbit coupling (SOC). SOC is known to split one van Hove singularity into two and also changes the topological nature of the Fermi surfaces. Hence, the presence of spin-orbit coupling gives the possibility of having high density of states in a large parameter space and additionally gives nontrivial topological band structures, providing a possible route to intrinsic topological superconductivity with large T_c. With recent progress in experimental techniques, it has now become possible to fabricate two-dimensional (2D) van der Waals materials [25–27] with high tunability both in doping or filling and spin-orbit coupling [28–31].

Motivated by this, we theoretically analyze the conditions under which topological superconductivity emerges in the Rashba-Hubbard model [32–39] in 2D, to capture the

---

*These two authors contributed equally.

simultaneous role of electronic correlations driven by Hubbard interaction, SOC within Rashba model, and singular density of states at van Hove singularities in 2D. Theoretically investigating interactions and singular density of states is challenging, since methods like mean-field or random-phase approximation calculations cannot capture the mutual interference between particle-particle and particle-hole instabilities at singularities [40], and quantum Monte Carlo applied to the Rashba-Hubbard model is plagued by the sign problem. We therefore employ the functional renormalization group (fRG) [41–43], which treats all instability channels on an equal footing, and augment it with a mean-field theory (MFT) in order to capture the nature of the superconductivity deep inside the phase.

Specifically, we find that while magnetism is suppressed by SOC, magnetic fluctuations near the van Hove singularities lead to A_1 and B_1 superconducting states, with dominant p- and d-wave-like pairing character, respectively, in a large parameter regime. Both of these pairing states exhibit nontrivial first-order topology [3] and host helical and flat-band Majorana edge states, respectively. Remarkably, we also find near the phase boundary between these two states a time-reversal breaking $A_1 + iB_1$ pairing state with higher-order topology and Majorana corner modes [44–52]. Furthermore, we extend the fRG + MFT method to real space, which allows us to deduce the topological and edge properties of the superconducting states, as well as the (in-)stabilities of the edge states against residual interactions, and the stability of these states to disorder. Our fRG + MFT approach in real space reveals that while both the helical Majorana and corner edge states are robust to residual interactions, the flat-band Majorana states are unstable towards the formation of a one-dimensional phase crystal [53–55]. We further find that the Majorana corner modes in the $A_1 + iB_1$ pairing state remain robust to disorder, defying the usual expectation that the sign-changing B_1 pairing, responsible for the corner modes, is sensitive to disorder.

Model and methods. We start from the Rashba-Hubbard Hamiltonian on the square lattice given by $H = H_0 + H_U$, with

$$H_0 = \sum_{j,j',\sigma} t_{jj'} c_{j,\sigma}^\dagger c_{j',\sigma} - \mu \sum_{j,\sigma} n_{j,\sigma}$$
$$+ i \sum_{\substack{j,j' \\ \sigma,\sigma'}} \lambda_{jj'} [(\mathbf{r}_j - \mathbf{r}_{j'}) \times c_{j,\sigma}^\dagger \vec{\tau}_{\sigma\sigma'} c_{j',\sigma'}]_z + \text{H.c.},$$

$$H_U = U \sum_j n_{j,\uparrow} n_{j,\downarrow}, \qquad (1)$$

where $c_{j,\sigma}$ ($c_{j,\sigma}^\dagger$) is the annihilation (creation) operator of an electron at site j with spin projection σ, $\vec{\tau}$ are the Pauli matrices, $\mathbf{r}_j$ is the lattice coordinate of site j, $n_{j,\sigma} = c_{j,\sigma}^\dagger c_{j,\sigma}$ is the spin-resolved particle number operator, and μ is the chemical potential. In the following, we choose the hopping amplitudes such that $t_{\langle j,j'\rangle} = -t$ when j and j' are nearest neighbors, $t_{\langle\langle j,j'\rangle\rangle} = -t'$ when j and j' are second neighbors, and zero otherwise. We set t as the energy unit. We also consider the Rashba SOC to be nonzero only for nearest neighbors $\lambda_{\langle j,j'\rangle} = \lambda t$. In the rest of the Letter, we take $\lambda = 0.3$. Results for different values of λ are shown in the Supplemental Material
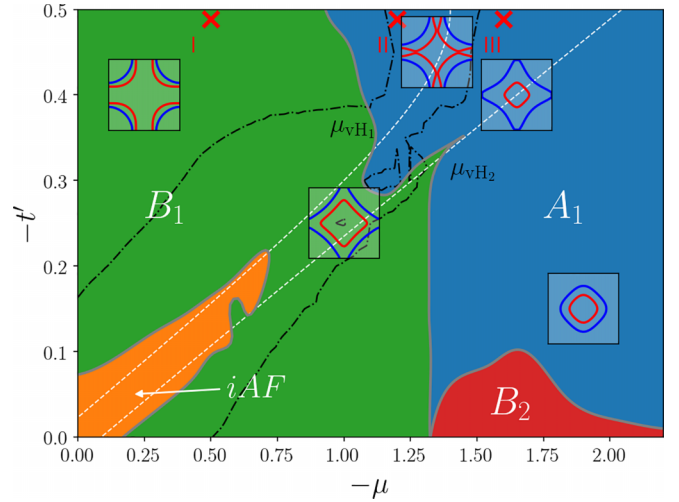
FIG. 1. Phase diagram of the Rashba-Hubbard model on the square lattice as a function of chemical potential μ and second-neighbor hopping t' for $U = 3t$. The dashed lines indicate the values of the chemical potentials $\mu_{\text{vH}_1}(t')$ and $\mu_{\text{vH}_2}(t')$ where the van Hove singularities VHS1 and VHS2 occur. The dashed-dotted lines enclose the region where T_c exceeds $10^{-6}t$.

(SM) [56] (see also Refs. [57–61] therein). We investigate the superconducting (SC) phases of the model in Eq. (1) by means of the fRG, combined with mean-field theory (fRG + MFT) [62–65]. This results in a renormalized superconducting gap equation of the form

$$\Delta_{\mathbf{k}}^{\sigma\sigma'} = \sum_{s,s'} \int_{\mathbf{k}'} \widetilde{V}_{\mathbf{k}\mathbf{k}'}^{\sigma\sigma'ss'} \left[T \sum_n F^{ss'}(\mathbf{k}', \nu_n) \right], \qquad (2)$$

where ν_n are fermionic Matsubara frequencies, T is the temperature, $\Delta_{\mathbf{k}}^{\sigma\sigma'}$ is the SC order parameter, and $F^{ss'}(\mathbf{k}', \nu_n)$ is the spin-resolved anomalous propagator, describing the propagation of a hole that gets reflected into a particle or vice versa. The function $\widetilde{V}_{\mathbf{k}\mathbf{k}'}^{\sigma\sigma'ss'}$ describes an effective interaction, computed by means of the fRG (see SM for details [56]). To determine the symmetry (and not the size) of the SC gap, we linearize Eq. (2) in $\Delta_{\mathbf{k}}^{\sigma\sigma'}$. The equation becomes, therefore, an eigenvalue problem, where the eigenvector corresponding to the largest positive eigenvalue gives the information on the symmetry of the leading superconducting state.

Phase diagram. In Fig. 1, we show the superconducting phase diagram as a function of chemical potential $\mu \leqslant 0$ and second-neighbor hopping $t' \leqslant 0$. We also show the different topologies of the two Fermi surfaces, as well as the lines along which the van Hove singularities of the two quasiparticle bands reach the Fermi level. We note that the density of states and position in k space of the two van Hove singularities are marked differently: VHS1 (left line) has a larger density of states than VHS2 (right line) and is also located further away from the $(\pi, 0)$ point (see SM [56]). In the orange region of Fig. 1, labeled as iAF, the fRG flow signals an (incommensurate) antiferromagnetic instability. In the region enclosed by the dashed-dotted black lines, the superconducting transition temperature exceeds $T = 10^{-6}t$, which is the lowest temperature accessible in our fRG computation.

A large portion of the phase diagram displays a leading superconducting state living in the B_1 representation of the combined spin-lattice symmetry group of Hamiltonian (1) [56]. The resulting gap function can, to leading order, be expressed as

$$\alpha_s(\cos k_x - \cos k_y)t^0 + \alpha_t(\sin k_y t^1 + \sin k_x t^2),$$

where $t^\mu = i\tau^\mu \tau^2$, and α_s and α_t are free parameters. Note that the singlet component of the gap (the one proportional to t^0) is the $d_{x^2-y^2}$-wave SC order parameter one would obtain in the Hubbard model without introducing SOC. Higher-order harmonics are considered in our calculations, but the effective attractions in the higher-order harmonic channels are found to be very small. At larger absolute values of the chemical potential, we obtain a phase belonging to the A_1 representation of the discrete symmetry group of the Hamiltonian. The SC gap in this state is a superposition of an extended s wave in the singlet component and a helical p wave in the triplet:

$$\alpha_s(\cos k_x + \cos k_y)t^0 + \alpha_t(-\sin k_y t^1 + \sin k_x t^2).$$

For larger $-\mu$ and small $-t'$, we also find a B_2 phase, characterized, however, by rather small values of the leading eigenvalue, resulting in low transition temperatures. The gap function in this phase is given by a dominant singlet component in the d_{xy} symmetry channel and a subdominant triplet part. We note that near the boundary between differently colored regions in Fig. 1 there is the possibility of a coexistence phase that combines the two order parameters (see discussion below). Hence, in general there will be two transitions as one goes from, e.g., deep inside the B_1 state to the A_1 state. Finally, we note that SOC disfavors ferromagnetic phases expected near van Hove singularities [24]. Instead, spin fluctuations drive the formation of the SC phases in a large-parameter regime even at van Hove fillings (see SM [56]).

Having identified different superconducting phases in Fig. 1, we then focus on each of them individually by investigating the characteristic points marked by red crosses in Fig. 1. Additionally, we extend the fRG + MFT method to real space to investigate the disorder stability of the phases and to determine possible interaction-induced edge instabilities [56]. Furthermore, we scale the interaction strengths by 10 in order to render the investigation of the edge properties on finite-size systems computationally amenable.

B_1 pairing state. In Fig. 2, we investigate the properties of the B_1 phase for the parameters marked by cross I ($\mu = -0.5$ and $t' = -0.5$) in Fig. 1. In this regime, the gap functions show (quasi-)nodes along the diagonal $k_x = \pm k_y$ (see SM [56]). This nodal structure suggests that a (11) edge is pair breaking [66,67] and will form a flat band of topological zero-energy states [2,68–70] protected by time-reversal symmetry and translational symmetry along (11). The large degeneracy of these zero-energy states makes them thermodynamically unstable and prone to symmetry breaking. To investigate the edge properties, we consider an open boundary geometry [see Fig. 2(a)] with one (11) edge. As shown in Fig. 2(a), at low temperatures, the (11) edge hosts oscillations in the phase θ of the d-wave superconducting order parameter, called phase crystals, breaking both time-reversal symmetry and translational symmetry along the (11) edge [53–55]. In comparison to earlier literature on phase crystals,
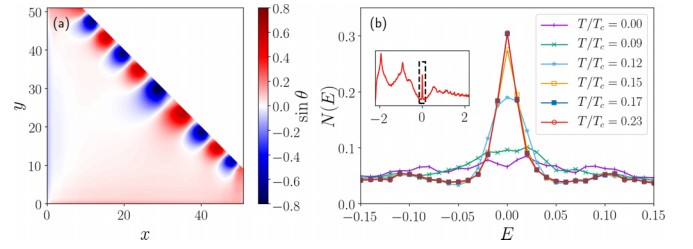
FIG. 2. (a) Phase crystal forming at the (11) edge. The sine of the phase θ of the d-wave superconducting order parameter is plotted in real space at $T = 0$ with the bulk value of $\sin\theta$ being subtracted. At the (11) edge there are clear modulations visible in $\sin\theta$. (b) Density of states $N(E)$ around zero energy for different temperatures T/T_c. The inset shows the density of states at $T/T_c = 0.23$ in a wider range.

one remarkable feature of the phase crystals obtained here is that they are robust to the additional presence of a subdominant triplet superconducting order parameter originating in the bulk due to SOC. We calculate the spatially averaged density of states $N(E) = 1/N \sum_{i,n,\sigma} |u_{i\sigma}^n|^2 \delta(E - E_n) + |v_{i\sigma}^n|^2 \delta(E + E_n)$, where N is the total number of lattice sites, and $u_{i\sigma}^n$ and $v_{i\sigma}^n$ are the eigenfunctions with eigenvalues E. To numerically evaluate $N(E)$, we use a Lorentzian with fixed width 0.01 to calculate the δ function. As shown in Fig. 2(b), $N(E)$ shows a large zero-bias peak for $T/T_c > 0.17$, showing the presence of a flat band of zero-energy states, which does not change with increasing temperature. Due to the formation of the phase crystal at $T/T_c \approx 0.17$, the zero-bias peak gets suppressed for lower temperatures since the phase crystals Doppler shift the zero-energy states to finite energies. With lowering temperature, the shift increases.

A_1 pairing state. We now investigate the topological edge states of the A_1 phase for the parameters marked by cross III ($\mu = -1.6$ and $t' = -0.5$) in Fig. 1. This A_1 pairing is a time-reversal symmetric fully gapped superconductor and belongs to the DIII class, characterized by a $\mathbb{Z}_2$ invariant in two dimensions [3]. In our case, there is one pocket around the M point with negative pairing and the system is topologically nontrivial according to $N_{2D} = \Pi_s [\text{sgn}(\Delta_s)]^{m_s}$, where m_s is the number of time-reversal invariant points enclosed by the sth Fermi surface [71]. Due to this nontrivial topology, we find helical edge states with open boundaries, shown in Sec. SVII of the SM [56].

$A_1 + iB_1$ pairing state. The transition from the B_1 superconducting state to the A_1 state with increasing $|\mu|$ in Fig. 1 gives the possibility of a coexisting phase where both order parameters are comparable. To explore this possibility, we fix the parameters to the values marked by cross II ($\mu = -1.2$ and $t' = -0.5$) in Fig. 1, which is near the phase boundary. Interestingly, we find a time-reversal symmetry-breaking $A_1 + iB_1$ superconducting phase as the lowest-energy state. To verify that the relative phase of $\pi/2$ between the A_1 and the B_1 order parameters is indeed the global minimum, we compare the condensation energies of the superconducting states with different relative phases ϕ. As shown in the inset of Fig. 3(a), $\phi = \pm\pi/2$ gives the largest condensation energy and consequently $A_1 \pm iB_1$ is the lowest in energy. Due to the imaginary B_1-pairing component, time-reversal symmetry and fourfold rotational symmetry C_4 are broken in this pairing state, but
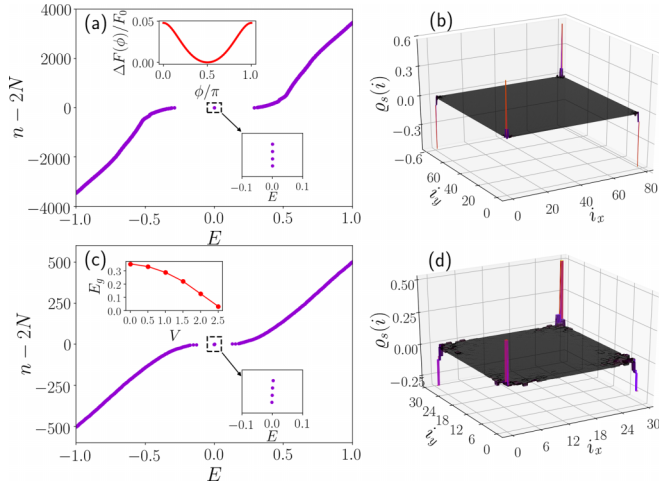
FIG. 3. (a) Eigenvalues with open boundary conditions along both x and y, showing four Majorana states. Upper inset: Normalized condensation energy ΔF as a function of the relative phase ϕ between A_1 and B_1 order parameters. Lower inset: Zoomed view of the four Majorana states. (b) Spin-projected wave function of the four Majorana states. (c), (d) Same as panels (a) and (b) but with disorder $V = 1.5$. Upper inset of panel (c): Bulk energy gap E_g as a function of the disorder strength V. Here, $T = 0$.

their combination is preserved, leading to a gap opening in the helical Majorana edge states. However, owing to the sign change of the B_1 pairing under C_4, the mass terms for adjacent edges [(10) and (01) edges] have opposite signs. Therefore, when these two edges meet at the corners, the mass term vanishes and Majorana corner modes are generated, realizing a second-order topological superconductor [44] (see SM [56]). To demonstrate this nontrivial topology, we study the corner states in a geometry with open boundary conditions along both the x and y directions. Similar to the A_1 phase, we only consider non-self-consistent eigenstates with open boundaries taking the fully self-consistent bulk solutions. Remarkably, we find four Majorana zero-energy states located in the superconducting gap, as shown in Fig. 3(a). The wave functions corresponding to these Majorana states are localized at the four corners (not shown). Spin characteristics of these Majorana states can be visualized by looking at the spin-projected wave functions $\varrho_s(i) = \sum_{\sigma n'} \text{sgn}(\sigma)(|u_{i\sigma}^{n'}|^2 + |v_{i\sigma}^{n'}|^2)$, where n' are the four zero-energy states. In Fig. 3(b), we see that $\varrho_s(i)$ is localized at the four corners with alternating signs for alternating corners. We have also verified the presence of Majorana corner states in a self-consistent calculation with edges for smaller system sizes. Therefore, the Majorana corner states in our numerical calculations confirm that the $A_1 + iB_1$ state is a higher-order topological superconductor.

To analyze the stability of the $A_1 + iB_1$ state to perturbations, we study the disorder effects on this phase. We introduce nonmagnetic chemical potential disorder by adding a term $H_V = \sum_i V_i n_i$ to the Hamiltonian, with V_i being a nonmagnetic impurity potential drawn from a random distribution, such that $V_i \in [-V/2, V/2]$ uniformly (i.e., Anderson disorder), and perform a fully self-consistent calculation. As shown in the inset of Fig. 3(c), the bulk gap E_g reduces with increasing disorder strength V, but remains finite for realistic

disorder strengths of $V \leqslant 2.0$. Notably, the average order parameters, shown in Fig. S4(c) of the SM [56], show more robust behavior. The disorder-robust behavior of $A_1 + iB_1$ is remarkable since the broken time-reversal symmetry makes Anderson's theorem [72] not applicable and might be related to the presence of interactions [73–76]. We also look at the corner states. Figures 3(c) and 3(d) show the eigenvalues and the spin-projected wave function of the lowest-energy states for $V = 1.5$. The Majorana corner states persist even in the presence of disorder, showing the stability of the higher-order topological superconductor. This finding is also striking from the following point of view. It is known that the topological nature of first-order topological phases makes Majoranas survive moderately strong disorder [77–79]. However, the corner modes in the higher-order $A_1 + iB_1$ arise due to the sign change of B_1 pairing at adjacent edges. Now, it is commonly believed that B_1 pairing is sensitive even to nonmagnetic disorder [80]. Hence, the persistence of Majorana corner modes in the presence of disorder is highly nonintuitive and opens a new way of understanding sensitivity of higher-order topological superconductors. It will also be interesting to investigate in the future the effects of other models of disorder.

Discussion. We have shown that the combined effects of van Hove singularities, Rashba SOC, and repulsive Hubbard interactions give rise to a cascade of topological superconducting states, including a nodal B_1 state (d-wave-like) with flat-band Majorana edge modes, a fully gapped A_1 state (p-wave-like) with helical Majorana edge modes, and a time-reversal breaking $A_1 + iB_1$ state with Majorana corner modes, which is also disorder-robust.

It is remarkable that we find interaction-driven topological superconducting phases in the vicinity of van Hove singularities due to the presence of SOC. We emphasize that the topological superconducting phases emerge robustly in the Rashba-Hubbard model, independent of the size of the Rashba SOC and survive the inclusion of further neighbor hoppings. The size of the Rashba SOC, however, decides the doping window where topological superconductivity is obtained. Although we have presented here only results for the square lattice, we expect these topological superconductors to arise also in other 2D lattices, e.g., the triangular or the honeycomb lattice, although with modified irreps, due to the different spin-lattice symmetry groups. While we have only considered effects of a Hubbard on-site interaction, longer-ranged interactions can bring in additional interesting aspects, which will be investigated in a future work. For example, on kagome lattice systems, nearest-neighbor interactions play a crucial role due to the sublattice interference effects [81,82].

Our results provide a guide to understand and design topological superconductivity in heavy-atom superlattices [83] and van der Waals materials [25–27]. The high variability of these materials may allow one to tune the Fermi level to the van Hove fillings, such that an intrinsic topological superconductor with large T_c can be realized. For example, in LAO/STO [84] or EuO/KTO [85] it is possible to tune the carrier density, and therefore the Fermi surface, by electric gating. With the recent progress in experimental techniques, the strength of the SOC can also be highly tuned. It can be tuned either by applying an electric field [28–31] or by changing the geometry of a superlattice. For example, SOC in the CeCoIn$_5$/YbCoIn$_5$

superlattices can be adjusted by the width of the YbCoIn$_5$ blocks [28,86]. In CeCoIn$_5$/YbCoIn$_5$ superlattices [28,86], there are already prospective signatures of topological superconductivity below $T_c \simeq 2$ K, a high value compared to the topological superconductivity proposed in semiconductor-superconductor nanowire devices [12,13]. Other promising candidates are van der Waals heavy-atom materials [87–89]. All these experimental developments and our findings taken together may open up a route to intrinsic topological superconductors being used for the design of quantum information devices. Moreover, the $A_1 + iB_1$ superconductor may show interesting diode [90,91] and piezoelectric effects [92], since it breaks both inversion and time-reversal symmetry.

[1] C. Beenakker, Annu. Rev. Condens. Matter Phys. **4**, 113 (2013).

[2] A. P. Schnyder and P. M. R. Brydon, J. Phys.: Condens. Matter **27**, 243201 (2015).

[3] C.-K. Chiu, J. C. Y. Teo, A. P. Schnyder, and S. Ryu, Rev. Mod. Phys. **88**, 035005 (2016).

[4] M. Sato and Y. Ando, Rep. Prog. Phys. **80**, 076501 (2017).

[5] M. M. Sharma, P. Sharma, N. K. Karn, and V. P. S. Awana, Supercond. Sci. Technol. **35**, 083003 (2022).

[6] F. O. von Rohr, Chem. Mater. **35**, 9455 (2023).

[7] K. Flensberg, F. von Oppen, and A. Stern, Nat. Rev. Mater. **6**, 944 (2021).

[8] N. Hao and J. Hu, Natl. Sci. Rev. **6**, 213 (2019).

[9] X. Wu, R.-X. Zhang, G. Xu, J. Hu, and C.-X. Liu, in *Memorial Volume for Shoucheng Zhang* (World Scientific, Singapore, 2021), pp. 35–60.

[10] J.-X. Yin, Z. Wu, J.-H. Wang, Z.-Y. Ye, J. Gong, X.-Y. Hou, L. Shan, A. Li, X.-J. Liang, X.-X. Wu *et al.*, Nat. Phys. **11**, 543 (2015).

[11] D. Wang, L. Kong, P. Fan, H. Chen, S. Zhu, W. Liu, L. Cao, Y. Sun, S. Du, J. Schneeloch *et al.*, Science **362**, 333 (2018).

[12] V. Mourik, K. Zuo, S. M. Frolov, S. R. Plissard, E. P. A. M. Bakkers, and L. P. Kouwenhoven, Science **336**, 1003 (2012).

[13] M. Aghaee *et al.* (Microsoft Quantum), Phys. Rev. B **107**, 245423 (2023).

[14] J. P. Carbotte and F. Marsiglio, Electron-phonon superconductivity, in *The Physics of Superconductors*, edited by K. H. Bennemann, J. B. Ketterson (Springer, Berlin, Heidelberg, 2003).

[15] P. M. R. Brydon, S. Das Sarma, H.-Y. Hui, and J. D. Sau, Phys. Rev. B **90**, 184512 (2014).

[16] O. Can, T. Tummuru, R. P. Day, I. Elfimov, A. Damascelli, and M. Franz, Nat. Phys. **17**, 519 (2021).

[17] W. Kohn and J. M. Luttinger, Phys. Rev. Lett. **15**, 524 (1965).

[18] R. Nandkishore, L. S. Levitov, and A. V. Chubukov, Nat. Phys. **8**, 158 (2012).

[19] J. González and T. Stauber, Phys. Rev. Lett. **122**, 026801 (2019).

[20] S. Blundell, *Magnetism in Condensed Matter*, Oxford Master Series in Condensed Matter Physics 4 (Oxford University, Oxford, 2001).

[21] A. L. Sharpe, E. J. Fox, A. W. Barnard, J. Finney, K. Watanabe, T. Taniguchi, M. A. Kastner, and D. Goldhaber-Gordon, Science **365**, 605 (2019).

[22] M. Fleischmann, R. Gupta, F. Wullschläger, S. Theil, D. Weckbecker, V. Meded, S. Sharma, B. Meyer, and S. Shallcross, Nano Lett. **20**, 971 (2020).

[23] D. Fay and J. Appel, Phys. Rev. B **22**, 3173 (1980).

[24] C. Honerkamp and M. Salmhofer, Phys. Rev. B **64**, 184516 (2001).

[25] K. S. Novoselov, A. Mishchenko, A. Carvalho, and A. H. C. Neto, Science **353**, aac9439 (2016).

[26] Y. Liu, N. O. Weiss, X. Duan, H.-C. Cheng, Y. Huang, and X. Duan, Nat. Rev. Mater. **1**, 16042 (2016).

[27] R. Bian, C. Li, Q. Liu, G. Cao, Q. Fu, P. Meng, J. Zhou, F. Liu, and Z. Liu, Natl. Sci. Rev. **9**, nwab164 (2022).

[28] M. Shimozawa, S. K. Goh, R. Endo, R. Kobayashi, T. Watashige, Y. Mizukami, H. Ikeda, H. Shishido, Y. Yanase, T. Terashima *et al.*, Phys. Rev. Lett. **112**, 156404 (2014).

[29] Z. Liu, Y.-X. Wang, Y.-H. Fang, S.-X. Qin, Z.-M. Wang, S.-D. Jiang, and S. Gao, Natl. Sci. Rev. **7**, 1557 (2020).

[30] Y. Zhang, F. Xue, C. Tang, J. Li, L. Liao, L. Li, X. Liu, Y. Yang, C. Song, and X. Kou, ACS Nano **14**, 17396 (2020).

[31] M.-G. Kang, J.-G. Choi, J. Jeong, J. Y. Park, H.-J. Park, T. Kim, T. Lee, K.-J. Kim, K.-W. Kim, J. H. Oh *et al.*, Nat. Commun. **12**, 7111 (2021).

[32] A. Greco and A. P. Schnyder, Phys. Rev. Lett. **120**, 177002 (2018).

[33] A. Greco, M. Bejas, and A. P. Schnyder, Phys. Rev. B **101**, 174420 (2020).

[34] R. Ghadimi, M. Kargarian, and S. A. Jafari, Phys. Rev. B **99**, 115122 (2019).

[35] S. Wolf and S. Rachel, Phys. Rev. B **102**, 174512 (2020).

[36] K. Nogaki and Y. Yanase, Phys. Rev. B **102**, 165114 (2020).

[37] M. Biderang, M.-H. Zare, and J. Sirker, Phys. Rev. B **105**, 064504 (2022).

[38] M. Kawano and C. Hotta, Phys. Rev. B **107**, 045123 (2023).

[39] J. Beyer, J. B. Profe, L. Klebl, T. Schwemmer, D. M. Kennes, R. Thomale, C. Honerkamp, and S. Rachel, Phys. Rev. B **107**, 125115 (2023).

[40] H. J. Schulz, Europhys. Lett. **4**, 609 (1987).

[41] P. Kopietz, L. Bartosch, and F. Schütz, *Introduction to the Functional Renormalization Group* (Springer, Berlin, 2010).

[42] W. Metzner, M. Salmhofer, C. Honerkamp, V. Meden, and K. Schönhammer, Rev. Mod. Phys. **84**, 299 (2012).

[43] J. Lichtenstein, D. Sánchez de la Peña, D. Rohe, E. Di Napoli, C. Honerkamp, and S. A. Maier, Comput. Phys. Commun. **213**, 100 (2017).

[44] Y. Wang, M. Lin, and T. L. Hughes, Phys. Rev. B **98**, 165144 (2018).

[45] Z. Yan, F. Song, and Z. Wang, Phys. Rev. Lett. **121**, 096803 (2018).

[46] Q. Wang, C.-C. Liu, Y.-M. Lu, and F. Zhang, Phys. Rev. Lett. **121**, 186801 (2018).

[47] X. Wu, X. Liu, R. Thomale, and C.-X. Liu, Natl. Sci. Rev. **9**, nwab087 (2022).

[48] Y.-T. Hsu, W. S. Cole, R.-X. Zhang, and J. D. Sau, Phys. Rev. Lett. **125**, 097001 (2020).

[49] M. Kheirkhah, Z. Yan, Y. Nagai, and F. Marsiglio, Phys. Rev. Lett. **125**, 017001 (2020).

[50] X. Wu, W. A. Benalcazar, Y. Li, R. Thomale, C.-X. Liu, and J. Hu, Phys. Rev. X **10**, 041014 (2020).

[51] S. Ikegaya, W. B. Rui, D. Manske, and A. P. Schnyder, Phys. Rev. Res. **3**, 023007 (2021).

[52] T. Li, M. Geier, J. Ingham, and H. D. Scammell, 2D Mater. **9**, 015031 (2022).

[53] M. Håkansson, T. Löfwander, and M. Fogelström, Nat. Phys. **11**, 755 (2015).

[54] P. Holmvall, M. Fogelström, T. Löfwander, and A. B. Vorontsov, Phys. Rev. Res. **2**, 013104 (2020).

[55] D. Chakraborty, T. Löfwander, M. Fogelström, and A. M. Black-Schaffer, npj Quantum Mater. **7**, 44 (2022).

[56] See Supplemental Material, which contains Refs. [24,42,93–97], at http://link.aps.org/supplemental/10.1103/PhysRevB.109.L180509 for details on the fRG + MFT method, the symmetry classification of the superconducting states, the real-space MF theory, the topological edge and corner states, the magnetic fluctuations, the results for different parameter choices, the disorder effects, and the momentum dependence of the gap functions.

[57] C. Husemann and M. Salmhofer, Phys. Rev. B **79**, 195125 (2009).

[58] W.-S. Wang, Y.-Y. Xiang, Q.-H. Wang, F. Wang, F. Yang, and D.-H. Lee, Phys. Rev. B **85**, 035414 (2012).

[59] C. Husemann, K.-U. Giering, and M. Salmhofer, Phys. Rev. B **85**, 075121 (2012).

[60] D. Vilardi, C. Taranto, and W. Metzner, Phys. Rev. B **96**, 235110 (2017).

[61] N. Dupuis, L. Canet, A. Eichhorn, W. Metzner, J. Pawlowski, M. Tissier, and N. Wschebor, Phys. Rep. **910**, 1 (2021).

[62] J. Wang, A. Eberlein, and W. Metzner, Phys. Rev. B **89**, 121116(R) (2014).

[63] H. Yamase, A. Eberlein, and W. Metzner, Phys. Rev. Lett. **116**, 096402 (2016).

[64] D. Vilardi, P. M. Bonetti, and W. Metzner, Phys. Rev. B **102**, 245128 (2020).

[65] P. M. Bonetti, Phys. Rev. B **102**, 235160 (2020).

[66] S. Kashiwaya and Y. Tanaka, Rep. Prog. Phys. **63**, 1641 (2000).

[67] T. Löfwander, V. S. Shumeiko, and G. Wendin, Supercond. Sci. Technol. **14**, R53 (2001).

[68] S. Ryu and Y. Hatsugai, Phys. Rev. Lett. **89**, 077002 (2002).

[69] M. Sato, Y. Tanaka, K. Yada, and T. Yokoyama, Phys. Rev. B **83**, 224511 (2011).

[70] A. P. Schnyder, C. Timm, and P. M. R. Brydon, Phys. Rev. Lett. **111**, 077001 (2013).

[71] X.-L. Qi, T. L. Hughes, and S.-C. Zhang, Phys. Rev. B **81**, 134508 (2010).

[72] P. Anderson, J. Phys. Chem. Solids **11**, 26 (1959).

[73] A. Garg, M. Randeria, and N. Trivedi, Nat. Phys. **4**, 762 (2008).

[74] D. Chakraborty and A. Ghosal, New J. Phys. **16**, 103018 (2014).

[75] D. Chakraborty, N. Kaushal, and A. Ghosal, Phys. Rev. B **96**, 134518 (2017).

[76] A. Ghosal, D. Chakraborty, and N. Kaushal, Phys. B (Amsterdam, Neth.) **536**, 867 (2018).

[77] R. Queiroz and A. P. Schnyder, Phys. Rev. B **89**, 054501 (2014).

[78] R. Queiroz and A. P. Schnyder, Phys. Rev. B **91**, 014202 (2015).

[79] Y. Lu, P. Virtanen, and T. T. Heikkilä, Phys. Rev. B **102**, 224510 (2020).

[80] H. Alloul, J. Bobroff, M. Gabay, and P. J. Hirschfeld, Rev. Mod. Phys. **81**, 45 (2009).

[81] M. L. Kiesel and R. Thomale, Phys. Rev. B **86**, 121105(R) (2012).

[82] X. Wu, T. Schwemmer, T. Müller, A. Consiglio, G. Sangiovanni, D. Di Sante, Y. Iqbal, W. Hanke, A. P. Schnyder, M. M. Denner *et al.*, Phys. Rev. Lett. **127**, 177001 (2021).

[83] M. Shimozawa, S. K. Goh, T. Shibauchi, and Y. Matsuda, Rep. Prog. Phys. **79**, 074503 (2016).

[84] A. D. Caviglia, S. Gariglio, N. Reyren, D. Jaccard, T. Schneider, M. Gabay, S. Thiel, G. Hammerl, J. Mannhart, and J. M. Triscone, Nature (London) **456**, 624 (2008).

[85] C. Liu, X. Yan, D. Jin, Y. Ma, H.-W. Hsiao, Y. Lin, T. M. Bretz-Sullivan, X. Zhou, J. Pearson, B. Fisher *et al.*, Science **371**, 716 (2021).

[86] Y. Mizukami, H. Shishido, T. Shibauchi, M. Shimozawa, S. Yasumoto, D. Watanabe, M. Yamashita, H. Ikeda, T. Terashima, H. Kontani *et al.*, Nat. Phys. **7**, 849 (2011).

[87] B. G. Jang, C. Lee, J.-X. Zhu, and J. H. Shim, npj 2D Mater Appl. **6**, 80 (2022).

[88] H. Hegger, C. Petrovic, E. G. Moshopoulou, M. F. Hundley, J. L. Sarrao, Z. Fisk, and J. D. Thompson, Phys. Rev. Lett. **84**, 4986 (2000).

[89] V. Posey *et al.*, APS March Meeting 2023, https://meetings.aps.org/Meeting/MAR23/Session/G29.5 (2023).

[90] F. Ando, Y. Miyasaka, T. Li, J. Ishizuka, T. Arakawa, Y. Shiota, T. Moriyama, Y. Yanase, and T. Ono, Nature (London) **584**, 373 (2020).

[91] A. Daido, Y. Ikeda, and Y. Yanase, Phys. Rev. Lett. **128**, 037001 (2022).

[92] M. Chazono, H. Watanabe, and Y. Yanase, Phys. Rev. B **105**, 024509 (2022).

[93] C. Wetterich, Phys. Lett. B **301**, 90 (1993).

[94] G. A. H. Schober, J. Ehrlich, T. Reckling, and C. Honerkamp, Front. Phys. **6**, 32 (2018).

[95] C. Platt, W. Hanke, and R. Thomale, Adv. Phys. **62**, 453 (2013).

[96] J. Zhu, *Bogoliubov-de Gennes Method and Its Applications*, Lecture Notes in Physics (Springer, Cham, Switzerland, 2016).

[97] A. P. Schnyder, P. M. R. Brydon, and C. Timm, Phys. Rev. B **85**, 024522 (2012).